

A Weakly Nonlinear Primitive Equation Baroclinic Life Cycle

STEVEN B. FELDSTEIN

Cooperative Institute for Research in the Environmental Sciences, University of Colorado, Boulder, Colorado

(Manuscript received 19 December 1992, in final form 8 April 1993)

ABSTRACT

A weakly nonlinear baroclinic life cycle is examined with a spherical, multilevel, primitive equation model. The structure of the initial zonal jet is chosen so that the disturbance grows very slowly, that is, linear growth rate less than 0.1 day^{-1} , and the life cycles of the disturbance are characterized by baroclinic growth and followed by barotropic decay. It is found that if the disturbance grows sufficiently slowly, the decay is baroclinic. As a result, the procedure for determining this weakly nonlinear jet is rather delicate.

The evolution of the disturbance is examined with Eliassen–Palm flux diagrams, which illustrate that the disturbance is bounded at all times by its critical surface in the model's middle and upper troposphere. The disturbance undergoes two large baroclinic growth/barotropic decay life cycles, after which it decays by horizontal diffusion. At the end of the first cycle, the zonally averaged zonal flow is linearly stable, suggesting that the disturbance growth during the second cycle may have arisen through nonmodal instability. This stabilization of the disturbance is due to an increase in the horizontal shear of the zonal wind, that is, the barotropic governor mechanism. It is argued that this stabilization is due to the large number of model levels.

A quasigeostrophic refractive index is used to interpret the result that as the linear growth rate of the disturbance is lowered, the ratio of equatorward to poleward wave activity propagation decreases. A parameter is defined as the ratio of the horizontal zonal wind shear to the Eady growth rate. It is found that the growing disturbance tends to be confined to regions of local minima of this parameter.

1. Introduction

Most studies of baroclinic life cycles have used models that fall into one of two general classes. The first class is represented by weakly nonlinear, two-layer, β -plane quasigeostrophic models. The second class is characterized by strongly nonlinear, multilevel, spherical, primitive equation models. Each class possesses its own distinct advantages and disadvantages. The primary advantage of class 1 models is that the results are usually easier to interpret, as simple linear diagnostics and conservation laws are applicable. However, even though this model is capable of simulating many aspects of the observed life cycles, some features of its baroclinic wave evolution are unrealistic. On the other hand, class 2 models capture many of the details of the observed baroclinic life cycles that the class 1 models cannot, but the additional complexity of class 2 models renders the results more difficult to interpret.

Examples of investigations that use class 1 models are Pedlosky (1970, 1971, 1981), Pedlosky and Frenzen (1980), Feldstein and Held (1989, FH hereafter), and Feldstein (1991, F hereafter). In the studies of Pedlosky, where the initial zonal flow is uniform, the disturbance always remains close to its normal-mode form and life cycles consist of baroclinic growth and

baroclinic decay. On the other hand, in FH, it was shown that if the meridional shear of the jet is sufficiently strong to produce a critical latitude, the disturbance undergoes significant changes in its structure and the life cycles are characterized by baroclinic growth followed by barotropic decay, as is seen in the atmosphere.

Calculations with class 2 models have been performed by many authors, including Gall (1976), Simmons and Hoskins (1978, 1980), McVean and James (1986), Thorncroft and Hoskins (1990), Branscome et al. (1989), Haynes and Shepherd (1989), Polavarapu and Peltier (1990), and Barnes and Young (1992). Two of the most important early studies were those of Gall and Simmons and Hoskins (1978). Gall was the first to model a baroclinic life cycle and show how the structure of the disturbance evolves from its linear growth stage, where it has its maximum amplitude near the lower boundary, to later times, where the maximum amplitude is in the upper troposphere. Simmons and Hoskins (1978) extended Gall's results to show that a disturbance decays barotropically just as rapidly as it grows baroclinically. Their entire baroclinic life cycle did capture many of the dominant features observed in the atmosphere.

There are several differences between the solutions from class 1 and class 2 models. For example, the class 1 solutions of FH and F find just a single cycle of growth and decay, whereas most class 2 solutions, for example,

Corresponding author address: Dr. Steven B. Feldstein, CIRES, University of Colorado, Campus Box 449, Boulder, CO 80309-0449.

McVean and James (1986) and Barnes and Young (1992), find two or more cycles. In addition, the two classes of models are expected to show different stabilization mechanisms for the growing disturbance. As is shown in FH and F for weakly nonlinear two-layer quasigeostrophic models, the disturbance is stabilized by removing the initial negative meridional potential vorticity gradient (Charney–Stern theorem) in the lower layer and replacing it with a value close to zero. On the other hand, in class 2 models with a sufficiently large number of levels, stabilization requires that the lowest-level meridional potential temperature gradient be removed everywhere (this stabilization criterion is strictly valid only for a vertically continuous quasigeostrophic fluid; nevertheless, in practice, it does seem to remain applicable to multilevel primitive equation models), which is impossible, as the disturbance can only move potential temperature contours at this level from one location to another. Also, class 1 models cannot stabilize the baroclinic waves by increasing the static stability, since the static stability must remain fixed. An increase in static stability was shown to be an important mechanism for the stabilization of baroclinic waves (see Gall 1976; Gutowski et al. 1989) in primitive equation models. A related mechanism is the so-called barotropic governor (see James and Gray 1986; James 1987), where horizontal shear of the zonal wind has been found to influence stabilization. In class 1 models, the change in the horizontal zonal wind shear is very small, whereas in class 2 models it is substantially larger. Another difference between the models involves the ratio of equatorward to poleward propagation of wave activity. In class 1 models, if the unstable jet is symmetric about its center, the amount of wave activity propagation is equal in both directions. On the other hand, in class 2 models with a symmetric jet—for example, Simmons and Hoskins (1978) and Barnes and Young (1992)—the majority of the wave activity propagates toward the equator. Furthermore, FH and F showed that the disturbance is always bounded by its critical latitudes. The question of whether critical latitudes play a similar role in class 2 models has not been completely addressed.

The purpose of this study is to try to better understand the differences between the solutions found in class 1 and class 2 models through the use of a model that combines the properties of both classes of models. Clearly, there are several combinations of model characteristics that can be constructed for this purpose, but one particular combination can be especially advantageous. This is a spherical, multilevel, primitive equation model that is *weakly nonlinear*. This model retains most of the characteristics of the class 2 models, yet it keeps the weak nonlinearity, which can give much simpler solutions to interpret, allowing additional insight into the properties of the much more realistic class 2 models. Thus, in order to avoid some of the limitations of class 1 models and yet retain the relative

simplicity of a weakly nonlinear model, a spherical, multilevel, primitive equation model will be used to examine a weakly nonlinear baroclinic life cycle.

In section 2, the model and the initial state will be described. The results will be presented in section 3 and the conclusions in section 4.

2. Model description

For this study, an equally spaced sigma-level, sector, primitive equation model is used. The model, developed by Isaac Held of the Geophysical Fluid Dynamics Laboratory (GFDL), is very similar to that of a GFDL general circulation model without the physical parameterizations. In a series of tests, it was found that the weakly nonlinear solution is convergent if more than 15 vertical levels and a horizontal resolution greater than rhomboidal 30 is used. As a result, and after considering computational constraints, a resolution of 20 vertical levels at rhomboidal 60 was selected. The model's zonal wavenumber spectrum consists of the fundamental, which is the fastest-growing zonal wavenumber, and its first four higher harmonics. To integrate the model, a semi-implicit scheme is used with a Robert filter and a time step of 0.02 days. In addition, friction is represented as eight-order horizontal diffusion, which is used to simulate the enstrophy cascade to subgrid scales. Other forms of forcing and dissipation, such as thermal forcing and surface heat fluxes and drag, are not included in the model runs, in order to study the baroclinic life cycles in their simplest context. These dissipation mechanisms have been shown by Branscome et al. (1989) and Barnes and Young (1992) to modify the low-level structure and stability characteristics of the disturbance and to allow for repeating life cycles. The value of the horizontal diffusion coefficient is $\nu = 3.2 \times 10^{35} \text{ m}^8 \text{ s}^{-1}$. This value for ν is small enough so that only the smallest meridional scales in the model are affected by the horizontal diffusion.

In this investigation, a weakly nonlinear jet is simply defined as a jet that is unstable to a very slowly growing disturbance, that is, the disturbance growth rate being at least an order of magnitude smaller than is typically observed in the atmosphere, which it usually about 1 day^{-1} . Because the selection of a weakly nonlinear initial state is found to be a very delicate problem, a detailed discussion of the model and in particular the initial state is presented. The initial zonally averaged temperature field is specified as

$$T(\theta, \sigma) = [T(\sigma)] + 2U_0(\sigma_0 a f / R)(H / \sigma_z)g(\theta)h(\sigma), \quad (2.1a)$$

where

$$g(\theta) = \tanh[(\theta - \theta_0) / \sigma_\theta], \quad (2.1b)$$

$$h(\sigma) = \text{sech}^2[-H(\ln \sigma - \ln \sigma_0) / \sigma_z] \\ \times \tanh[-H(\ln \sigma - \ln \sigma_0) / \sigma_z], \quad (2.1c)$$

and θ and σ are the meridional and vertical coordinates, respectively. This temperature field is symmetric about the equator. The parameters in (2.1a,b,c) have the following definitions: H is the scale height, U_0 a measure of the speed of the jet maxima, a the earth's radius, f the Coriolis parameter, R the gas constant, σ_θ and σ_z the jet half-width in the horizontal and vertical directions, respectively, and θ_0 and σ_0 the latitude and sigma value of the jet maxima, respectively. The choices of values for the above model parameters are shown in the Appendix.

After the zonally averaged temperature field is specified, a nonlinearly balanced initial zonally averaged zonal wind is determined. The secant method is used for calculating this balanced state. This technique is described in detail by Branscome et al. (1989). A balanced initial state is being used to suppress the initial presence of gravity waves. It is desirable to remove the gravity waves since in the present calculation the amplitude of the disturbance is unrealistically small and may be influenced by the gravity waves. The resulting zonally averaged initial temperature and zonal wind fields are shown in Fig. 1.

The values of the model parameters were chosen to select the baroclinically unstable jet that gives rise to the most slowly growing disturbance that retains a life cycle characterized by baroclinic growth and barotropic decay. For smaller linear growth rates, it was found that the disturbance undergoes a life cycle consisting of baroclinic growth and baroclinic decay. The key parameters that determine the growth rate of the disturbance were found to be U_0 and H/σ_z . The parameter U_0 , which measures the strength of the jet, equals the maximum zonal wind speed if the zonal wind precisely goes to zero at the top and bottom boundaries of the model. In the present model, this condition is not satisfied, and the actual maximum zonal wind speed equals about $0.75U_0$. The parameter H/σ_z controls the meridional temperature gradient of the model's lowest level. The lowest-level meridional temperature gradient can be reduced by selecting small values of H/σ_z . Therefore, the growth rate of the disturbance can be lowered by specifying smaller values for U_0 and H/σ_z .

Several problems arise when trying to find appropriate values for U_0 and H/σ_z . If these parameters are sufficiently small, as discussed above, the disturbance will grow and decay baroclinically. Furthermore, if these parameters are too large, a negative $\partial Q/\partial y$ region will exist between the level of the jet maxima and the lower boundary. This is not desirable as the aim of this study is to examine the life cycle that arises from a boundary and not an internal instability (James and Hoskins 1985; McVean and James 1986). This negative $\partial Q/\partial y$ region occurs because the initial state is chosen so that the vertical shear and curvature of the zonal jet are small at low levels, which in turn requires the vertical curvature of the jet to increase at higher levels. Thus, the choice of values for U_0 and H/σ_z is

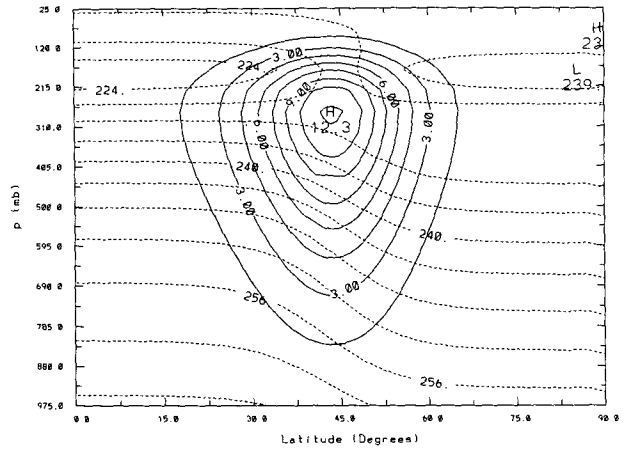


FIG. 1. Meridional cross section of the initial zonally averaged zonal wind (solid line) and temperature field (dashed line). The contour intervals are 1.5 m s^{-1} and 5 K , respectively.

somewhat delicate, as these parameters must be small enough to suppress internal instability below the jet maxima, but they must be large enough to ensure that the eventual decay of the disturbance will be barotropic.

In order to determine the values of U_0 and H/σ_z , a series of ten numerical integrations was performed. Each numerical integration was costly in terms of cpu time, as a 100 model day integration would take 3 h 20 min of cpu time on a Cray X/MP 28. Because of the limited number of numerical experiments, it was not possible to find the weakest possible jet that yields a baroclinic growth/barotropic decay life cycle. Nevertheless, the results from these integrations suggest that the initial state shown in Fig. 1 should be quite close to satisfying the above requirements. In addition, by calculating the quasigeostrophic meridional potential vorticity gradient (see Fig. 3), it was found that this particular initial state suppresses any internal instability.

In order to better understand why baroclinic decay can occur when U_0 and H/σ_z are small, it is helpful to look at the quasigeostrophic refractive index n^2 defined by Palmer (1982), modified for use in pressure coordinates by Randel and Stanford (1985), which is

$$n^2 = \left[\frac{\partial Q/\partial y}{U - \omega a \cos \theta} - \frac{f^2}{4H^2 N^2} - \frac{k^2}{a^2 \cos^2 \theta} \right] / \sin^2 \theta, \quad (2.2)$$

where U is the zonally averaged zonal wind, ω the angular velocity of the disturbance, N the Brunt-Väisälä frequency, and k the zonal wavenumber. The quasigeostrophic meridional potential vorticity gradient, $\partial Q/\partial y$, is defined as

$$\partial Q/\partial y = \frac{2\Omega \cos \theta}{a} + \frac{1}{a} \frac{\partial \zeta}{\partial \theta} - f^2 \frac{\partial}{\partial p} \left[\left(\frac{\rho g}{N} \right)^2 \frac{\partial U}{\partial p} \right], \quad (2.3)$$

where ζ is the zonally averaged relative vorticity, ρ the density, g the gravitational acceleration, and p pressure. The refractive index n^2 and $\partial Q/\partial y$ for the initial state are shown in Figs. 2 and 3, respectively. The zonal wavenumber and angular velocity, which are used for determining n^2 , are those values corresponding to the fastest growing zonal wavenumber. These values were found from a linear stability analysis of the initial state to be $k = 7$ and $\omega = 2.4 \times 10^{-7} \text{ s}^{-1}$. According to linear quasigeostrophic theory, regions of propagation (evanescence) are characterized by $n^2 > 0$ ($n^2 < 0$). In Fig. 2, the dark broad line indicates where n^2 attains its largest values. This line approximates the critical surface, defined as locations where $U - \omega a \cos \theta = 0$ (for a continuous flow n^2 would be infinite at the critical surface). In addition, turning levels, identified by $n^2 = 0$ contours, are present at a level above the jet maxima. For plane-parallel shear flows with $\partial Q/\partial y > 0$ everywhere, it is well known that linear quasigeostrophic disturbances are absorbed (reflected) at critical surfaces (turning levels).

One result found from the above series of numerical integrations was that in order for barotropic decay to occur, instead of baroclinic decay, the negative n^2 region above and poleward of the jet maxima has to be sufficiently negative, that is, $n^2 < -0.25 \times 10^{-13} \text{ m}^{-2}$. Through the use of (Eliassen-Palm) EP flux diagrams, it was found that the EP flux vectors could still cross $n^2 = 0$ contours but they would be refracted away from n^2 contours that were sufficiently negative. (For positive or slightly negative n^2 , the EP flux vectors would be reflected downward off a horizontal turning level near $p = 200$ mb, resulting in baroclinic decay.) Thus, although the quasigeostrophic refractive index is not precise, it is a useful indicator of the wave propagation characteristics. This negative n^2 region was specified by choosing the initial temperature field so that $\partial Q/\partial y$

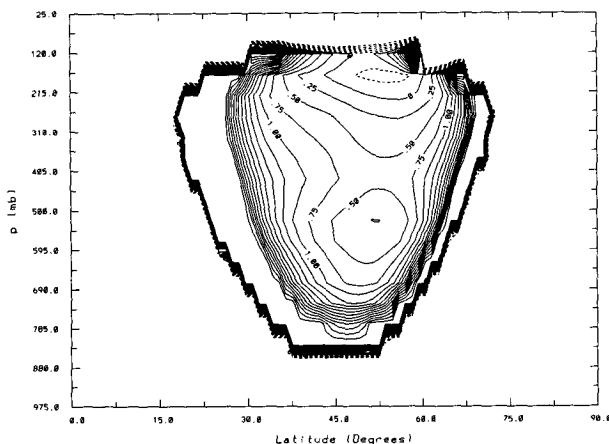


FIG. 2. Meridional cross section of the quasigeostrophic refractive index. Solid contours are positive and dashed contours negative. Contour interval is $2.5 \times 10^{-14} \text{ m}^{-2}$. The thick solid line denotes the approximate location of the critical surface.

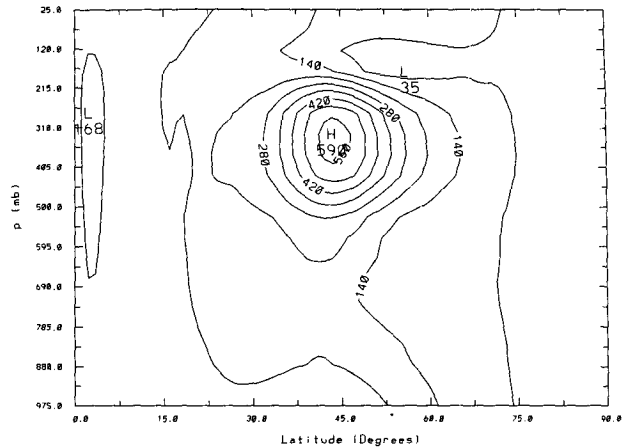


FIG. 3. Meridional cross section of the quasigeostrophic meridional potential vorticity gradient. Contour interval is $7.0 \times 10^{-12} \text{ m}^{-1} \text{ s}^{-1}$.

$\partial Q/\partial y$ is small, but still positive, to preclude internal instability. This is accomplished both by picking the upper-level [$T(\sigma)$] field to be warmer than observed, such that N^2 is increasing with height, and by choosing U_0 and H/σ_z to be large enough so that the thermal term in $\partial Q/\partial y$ [the third term on the right side of (2.3)] is negative in this region. These parameter specifications contribute to a negative $\partial Q/\partial y$ from the third term on the right side of (2.3) at all levels above the jet maxima. The second term on the right side of (2.3) is positive at the center of the jet and negative on both sides of the jet. The sum of all three terms in (2.3) then allows for $\partial Q/\partial y$ to be positive everywhere and shifts the $\partial Q/\partial y$ minimum, hence the negative n^2 region, to the poleward side of the jet.

The existence baroclinic decay was somewhat surprising. In F, where a critical layer was always present in the upper layer, it was found that baroclinic decay occurs only if the jet is very wide, that is, its width greater than or equal to 24 Rossby deformation radii. For such a wide jet, the refractive index is positive and increases in a direction outward from the center of the jet. In addition, the refractive index changes only slightly over the meridional extent of the disturbance. In this case, the critical layer, and thus the region where the refractive index is very large, is at a distance far from the disturbance so that critical-layer dynamics does not influence the evolution of the disturbance. As a result, meridional radiation of the disturbance is suppressed and the life cycle resembles the analytical solutions of Pedlosky (1970), where the basic state zonal wind is constant and the disturbance grows and decays baroclinically. When narrower jets were examined, F found larger changes in the refractive index over the meridional length of the disturbance. As a result, the disturbance did radiate meridionally toward its critical layers and barotropic decay occurred. In the present model, the refractive index does vary substantially over

the scale of the disturbance (the meridional extent of the perturbation can be seen in Fig. 4, which shows the amplitude of the perturbation streamfunction). As U_0 and H/σ_z are reduced from their values in Fig. 1, the width of the disturbance becomes smaller and the vertical structure of the refractive index is found to substantially change as the negative n^2 region is removed. For these smaller values of U_0 and H/σ_z , the horizontal turning of the EP flux vectors is suppressed since the disturbance first propagates upward and then back downward as it reflects off a horizontal turning level in the upper troposphere. Nevertheless, since the meridional variation of the refractive index remains large, as is the case for the narrower jets of the two-layer quasigeostrophic models, it is puzzling that baroclinic decay can occur in the present multilevel primitive equation model.

3. Results

In this section, the weakly nonlinear baroclinic life cycle will be examined in detail. The initial perturbation consists of the fastest-growing normal mode and its amplitude was chosen to be small enough so that changes to the initial zonally averaged zonal flow were very small after 30 days. The linear growth rate of this perturbation is 0.099 day^{-1} . The resulting energy cycle is calculated with the full primitive equation energetics of Lorenz (1955), and is shown in Fig. 5. These energies and their conversions are computed by integrating over the entire model atmosphere. The maximum total energy (the sum of the eddy kinetic and eddy available potential energies) attained by the disturbance is two orders of magnitude less than is typically observed in the atmosphere (see Randel and Stanford 1985). It can be seen that the disturbance undergoes two large amplitude cycles of baroclinic growth followed by

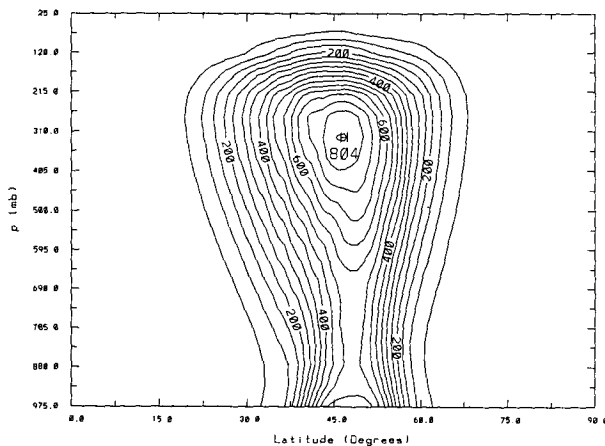


FIG. 4. Meridional cross section of the absolute value of the disturbance streamfunction during the linear growth stage. The maximum amplitude of the streamfunction is arbitrary. Contour interval is $5.0 \times 10^4 \text{ m}^2 \text{ s}^{-1}$.

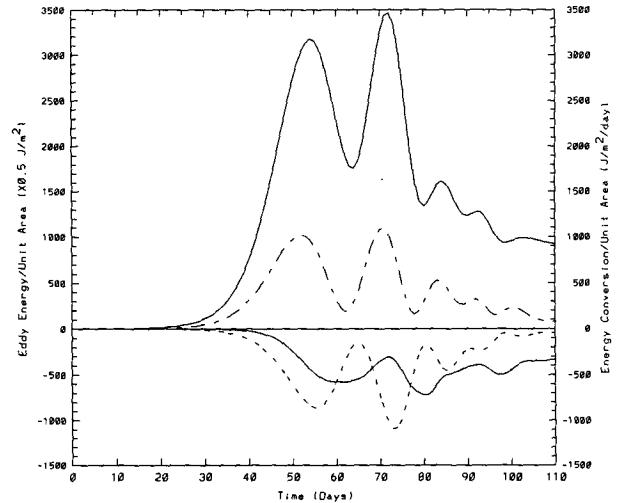


FIG. 5. Time series of total eddy energy (positive solid line), baroclinic energy conversion (long dashed/short dashed line), barotropic energy conversion (short dashed line), and dissipative energy conversion (negative solid line).

barotropic decay. The second cycle actually has a larger maximum energy than the first cycle. After the completion of these two cycles, the disturbance gradually dissipates through horizontal diffusion.

As discussed in the Introduction, most strongly nonlinear studies find two or more large amplitude cycles: for example, McVean and James (1986) and Barnes and Young (1992). However, other strongly nonlinear calculations find just a single cycle of growth and decay: for example, Simmons and Hoskins (1978). This single growth and decay cycle was shown by Barnes and Young to occur when the diffusion coefficient is sufficiently large. With regard to atmospheric observations, Randel and Stanford find that synoptic-scale baroclinic waves usually undergo two or three large amplitude cycles before they decay to a much smaller amplitude (see Figs. 10a and 10c of Randel and Stanford).

a. Eliassen-Palm flux diagnostics

In order to better understand the evolution of the disturbance, EP flux vectors and their divergence [see Edmon et al. (1980) for a detailed explanation of EP flux diagrams] are plotted at five-day intervals from day 40 through day 75 of the life cycle (see Fig. 6). This time period encompasses the two large amplitude cycles of growth and decay. The primitive equation form of the EP flux vector (see Andrews and McIntyre 1976) in pressure coordinates is used. In order to illustrate these diagrams on pressure surfaces, logarithmic interpolation from sigma to pressure coordinates was performed. This is written as $\mathbf{F} = (0, F^{(\theta)}, F^{(p)})$, where

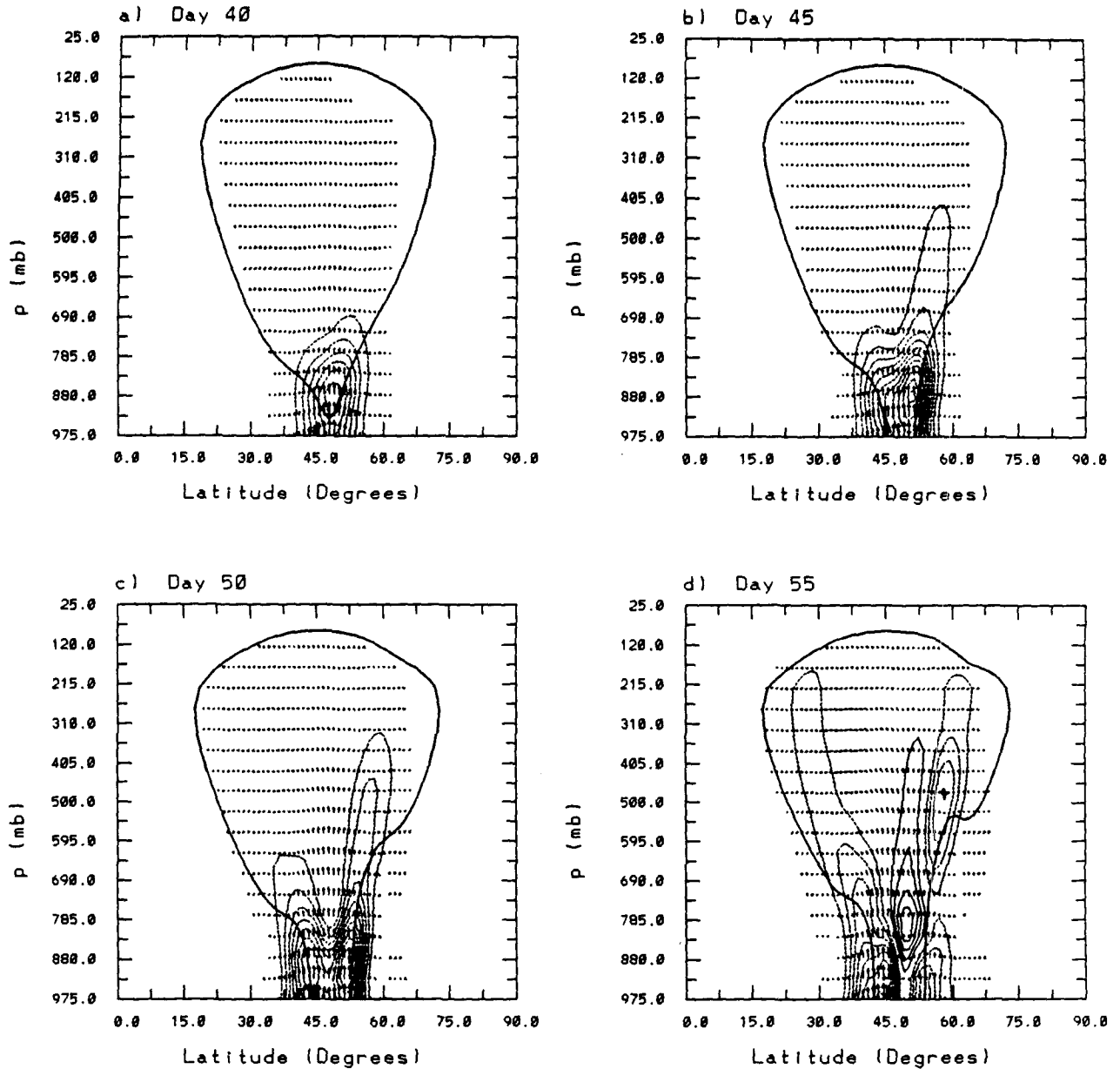


FIG. 6. Eliassen-Palm cross sections during the evolution of the disturbance for (a) day 40, (b) day 45, (c) day 50, (d) day 55, (e) day 60, (f) day 65, (g) day 70, and (h) day 75. The contours represent constant values of $\nabla \cdot \mathbf{F} / a \cos \theta$. Solid contours are positive and dashed contours negative. The contour interval for (a) is $1.0 \times 10^{-6} \text{ m s}^{-2}$, (b) $1.0 \times 10^{-6} \text{ m s}^{-2}$, (c) $1.0 \times 10^{-6} \text{ m s}^{-2}$, (d) $7.5 \times 10^{-7} \text{ m s}^{-2}$, (e) $5.0 \times 10^{-7} \text{ m s}^{-2}$, (f) $6.0 \times 10^{-7} \text{ m s}^{-2}$, (g) $6.0 \times 10^{-7} \text{ m s}^{-2}$, (h) $5.0 \times 10^{-7} \text{ m s}^{-2}$. The maximum vector length for (a) is 1.47×10^{13} ,

$$F^{(\theta)} = a \cos \theta \left(-\overline{u'v'} + \frac{\overline{v'\theta'}}{\partial \theta / \partial p} \overline{\partial U / \partial p} \right) \quad (3.1a)$$

$$F^{(p)} = a \cos \theta \left(\gamma \frac{\overline{v'\theta'}}{\partial \theta / \partial p} - \overline{u'w'} \right), \quad (3.1b)$$

where w is the vertical velocity in pressure coordinates, γ the absolute vorticity, and the overbar denotes a zonal average. The use of EP flux diagrams is well suited to the present weakly nonlinear calculation because \mathbf{F} is

parallel to the group velocity vector only for small amplitude disturbances.

The thick solid line in Fig. 6 indicates the location of the critical surface at that particular time. The disturbance angular velocity spectrum, which determines the location of the critical surface, is found in the following manner. At a specified time, the enstrophy for each spherical harmonic is calculated at every level. Then, those spherical harmonics whose enstrophy exceeds one-half the maximum enstrophy are identified.

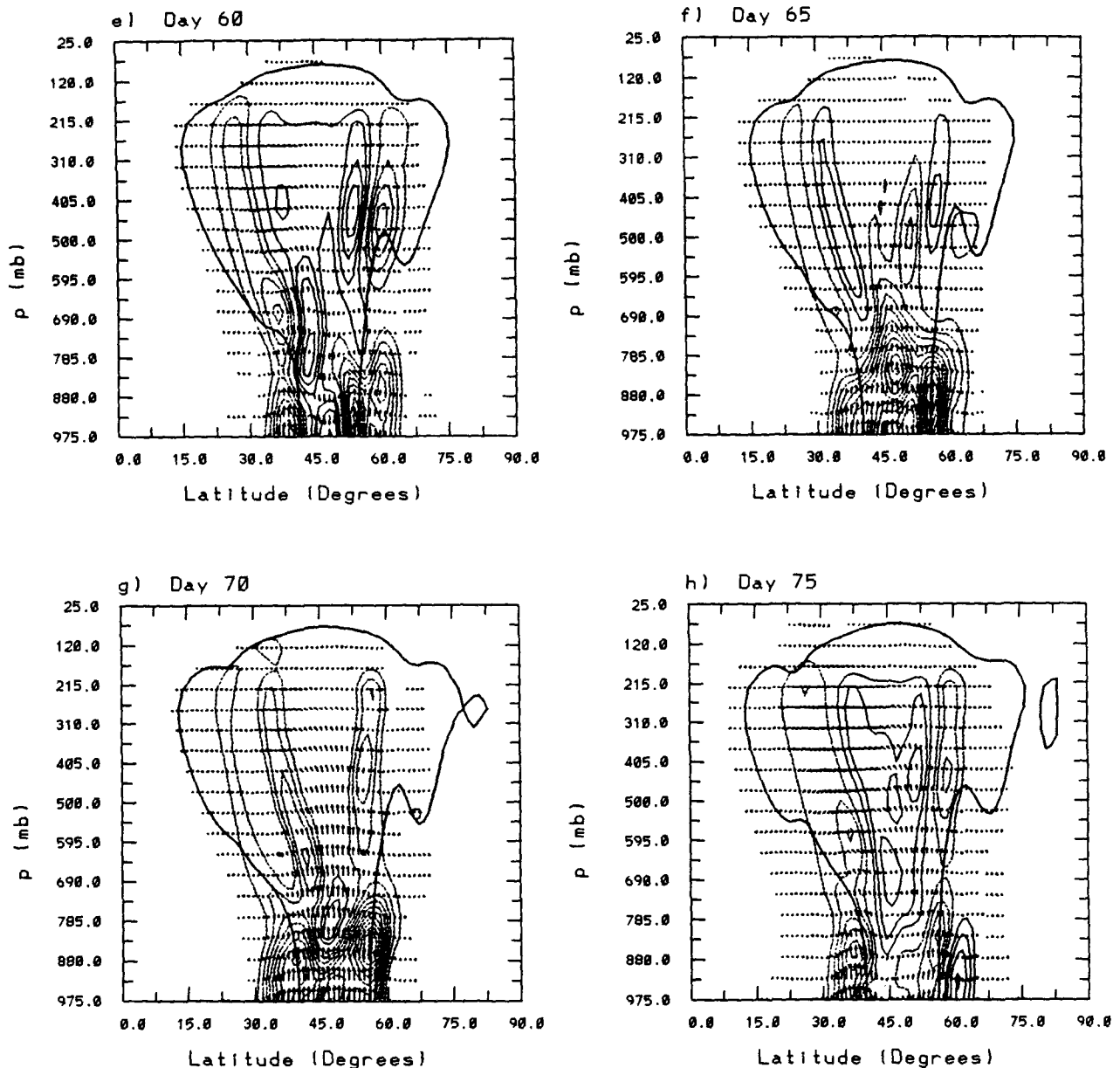


FIG. 6. (Continued) (b) 2.48×10^{13} , (c) 2.40×10^{13} , (d) 1.89×10^{13} , (e) 8.07×10^{12} , (f) 1.13×10^{13} , (g) 1.44×10^{13} , (h) 5.69×10^{12} . The thick solid line denotes the location of the critical surface, which is defined as $U - \omega a \cos \theta = 0$. The value of ω in (a) is $2.45 \times 10^{-7} \text{ s}^{-1}$, (b) $2.5 \times 10^{-7} \text{ s}^{-1}$, (c) $2.5 \times 10^{-7} \text{ s}^{-1}$, (d) $2.5 \times 10^{-7} \text{ s}^{-1}$, (e) $2.0 \times 10^{-7} \text{ s}^{-1}$, (f) $2.0 \times 10^{-7} \text{ s}^{-1}$, (g) $1.6 \times 10^{-7} \text{ s}^{-1}$, (h) $1.5 \times 10^{-7} \text{ s}^{-1}$.

This gives a spectrum of angular velocities. During the early stages of the life cycle, when the disturbance is growing linearly, the angular velocity spectrum is narrow. At later times, the angular velocity spectrum broadens. At all times, the thick solid line in Fig. 6 represents the minimum angular velocity.

At day 40, F is still close to its linearly unstable normal-mode form. The magnitude of F has a single maxima located slightly poleward of the jet. This is similar to the behavior found by Edmon et al. (1980), who use EP flux diagnostics to examine the strongly non-

linear life cycle solutions of Simmons and Hoskins (1978). The critical surface bounds the disturbance everywhere except near the lower boundary. At this time, the angular velocity spectrum is relatively narrow as $2.4 \times 10^{-7} \text{ s}^{-1} < \omega < 2.5 \times 10^{-7} \text{ s}^{-1}$. Next to the lower boundary, F crosses the critical surface. This behavior is consistent with the theory of critical-level overreflection [for a summary of critical-level overreflection and linear instability see Lindzen (1988)], which is strictly valid only for plane-parallel shear flows. From the viewpoint of critical-level overreflection, a

wave is first generated at the ground, where $\partial T/\partial y < 0$ and $\partial Q/\partial y$ takes on a negative delta function structure. The wave then tunnels through the region where $U - \omega a \cos \theta < 0$ and $n^2 < 0$, and is overreflected at the critical level. This leads to a downward-propagating wave that then reflects upward from the lower boundary [for linear baroclinic instability, see Snyder and Lindzen (1988)].

At day 45, $|\mathbf{F}|$ increases and the critical surface (at this time, the critical surface corresponds to $\omega = 2.5 \times 10^{-7}$) intersects the lower boundary. This lowering of the elevation of the critical surface seems to be inconsistent with critical-level overreflection. However, there is no inconsistency, as the necessary conditions for critical-level overreflections do indeed persist. This is because, unlike earlier times when the angular velocity spectrum remained very narrow at all levels, the angular velocity spectrum significantly broadens in the lowest two levels: at $\sigma = 0.925$, $2.5 \times 10^{-7} \text{ s}^{-1} < \omega < 4.7 \times 10^{-7} \text{ s}^{-1}$, and at $\sigma = 0.975$, $2.5 \times 10^{-7} \text{ s}^{-1} < \omega < 5.6 \times 10^{-7} \text{ s}^{-1}$. Thus, the disturbance propagates eastward at a faster speed and maintains the requirements of critical-level overreflection. To some extent, it is not surprising that these results remain consistent with critical-level overreflection as this theory is relevant for small amplitude disturbances in weakly unstable flows.

At day 50, two separate maxima in \mathbf{F} begin to form near the lower boundary, and by day 55, when the disturbance starts to decay, these two maxima in \mathbf{F} completely separate. Also, at day 55, there is stronger meridional radiation of wave activity at the upper levels, as indicated by the predominantly horizontal \mathbf{F} . In addition, at the same time, a region of positive $\nabla \cdot \mathbf{F}$ develops below the jet maxima. This positive $\nabla \cdot \mathbf{F}$ is found to coincide with the generation of a weak negative $\partial Q/\partial y$ (not shown), which arises from an increase in the vertical curvature of the zonal flow between the jet maxima and the lower boundary. By applying wave activity conservation (see Edmon et al.), the collocation of both negative $\partial Q/\partial y$ and positive $\nabla \cdot \mathbf{F}$ suggests that a weak internal instability has developed in this region.

The disturbance energy continues to decline at day 60. Between the two regions of upward \mathbf{F} on the lower boundary, the direction of \mathbf{F} has reversed and points downward. This indicates that the meridional heat flux is poleward at the wings of the jet and equatorward at the center of the jet.

The second cycle starts near day 65. The region of upward of \mathbf{F} is now about 50% wider than at the beginning of the first cycle. Furthermore, the remnants of the decaying disturbance of the first cycle are seen as the two weak dipoles in $\nabla \cdot \mathbf{F}$ on either side of the jet. At this time, the angular velocity spectrum is much broader than during the early stages of the first cycle, that is, $2.0 \times 10^{-7} \text{ s}^{-1} < \omega < 4.4 \times 10^{-7} \text{ s}^{-1}$, and the conditions for critical-level overreflection are no longer satisfied. This suggests that the growing disturbance at

the beginning of the second cycle is no longer a linearly unstable normal mode. In order to further test this idea, the linear stability of the zonally averaged flow at day 65 was examined. It was found that no linearly unstable modes were present. Since the meridional heat fluxes are poleward at day 65, this indicates that the disturbance is tilted westward with height and thus has the appropriate vertical structure to extract energy from the zonally averaged flow. This behavior indicates that during the second cycle, the disturbance may be growing via nonmodal instability (see Farrell 1982, 1984).

The disturbance continues to grow at day 70, and by day 75, as in the first cycle, it splits into two regions of upward \mathbf{F} and meridional radiation of wave activity characterizes its decay.

Throughout both cycles, \mathbf{F} always terminates before reaching the critical surface, which indicates that the wave activity is being absorbed by the background flow. In FH, it was found with a two-layer quasigeostrophic model that the disturbance is also absorbed before reaching its critical latitude. In addition, in contrast to the results of the present model where the angular velocity spectrum broadens with time, FH found that the upper-layer phase speed spectrum remains very narrow with a mean value very close to the initial linearly unstable phase speed. With the exception of the study of Barnes and Young (1992), all other strongly nonlinear life cycle studies do not address the question of whether the disturbance is bounded by its critical surface. In the model study of Barnes and Young, they showed that the potential vorticity fluxes on the 350-K isentropic surface decay to small value no farther than 10° latitude equatorward of the critical line, which they defined as the average phase speed of the disturbance. Thus, Barnes and Young found that the disturbance is approximately bounded by a latitude defined by the mean phase speed of the disturbance. In the present study, because of the broadening of the angular velocity spectrum, the critical surface was defined as the minimum in a wide spectrum of angular velocities. As a result, this particular critical surface gives a tighter bound than that obtained by Barnes and Young (see Fig. 6), and this bound applies over most of the domain except in the model's lower troposphere. These numerical results are consistent with those of the observational study of Randel and Held (1991) for both the Northern and Southern hemispheres. They find that the phase speeds of synoptic-scale eddies are almost always less than that of the time mean zonally averaged zonal winds.

An examination of \mathbf{F} indicates that wave activity propagates both equatorward and poleward during both cycles. The latitude that divides the equatorward and poleward propagation occurs at about 52°N . This is the same latitude at which the initial refractive index has a local minimum (see Fig. 2), that is, $\partial n/\partial \theta = 0$, and is consistent with linear wave propagation theory, where wave activity must propagate away from local

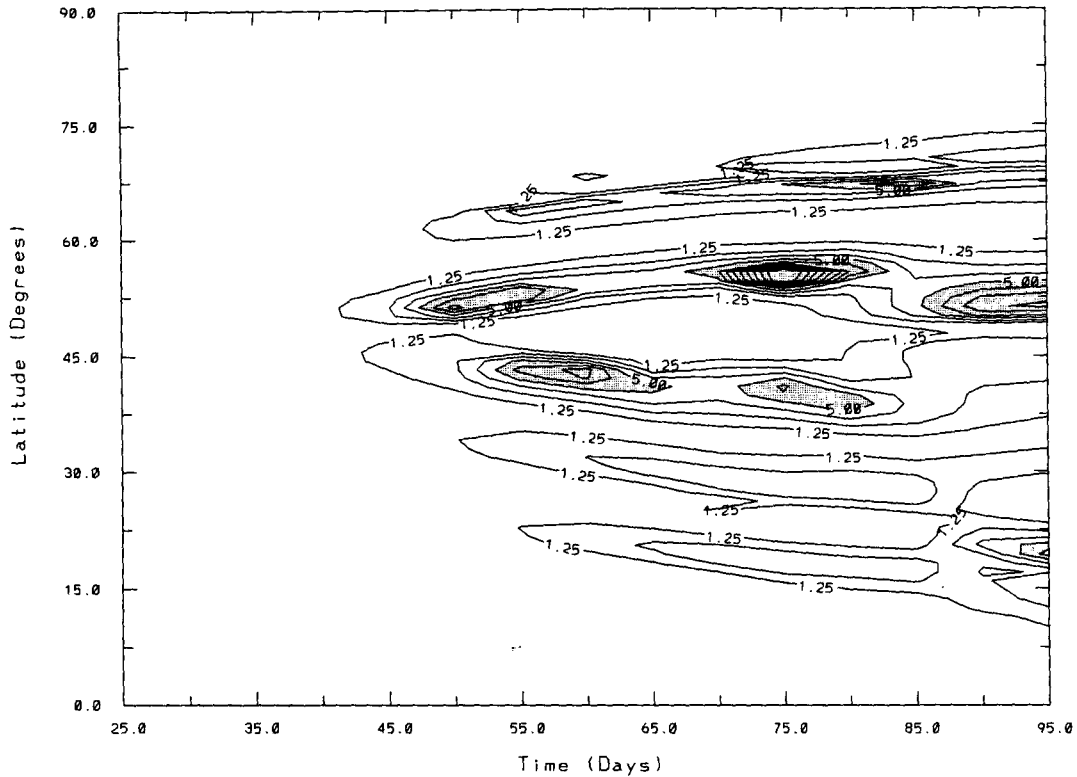


FIG. 7. Latitude-time contour diagram of the ratio of the lowest level horizontal shear $\partial U/\partial y$ to the Eady growth rate. Contour interval is 1.25. Shaded above 5.0.

minima in the refractive index. Similar behavior was found by Edmon et al. (1980), Hoskins (1983), and Barnes and Young (1992) for strongly nonlinear life-cycle calculations. However, in those calculations, a greater fraction of the wave activity propagates equatorward than is observed with the present weakly nonlinear model. An explanation for these model differences can be obtained by further examining the refractive index. In Fig. 2, as stated above, $\partial n/\partial \theta = 0$ at about 52°N , and at a latitude near 48°N , the initial disturbance reaches its maximum amplitude (see Fig. 4). If we assume that the amount of wave activity generated is symmetric about the latitude of the disturbance's maximum amplitude, there should be a slight preference for equatorward wave activity propagation. For a strongly nonlinear jet, the refractive index was calculated with the same parameters as in Fig. 1, except U_0 was increased so that the maximum zonal wind speed was 40 m s^{-1} . In this calculation, the latitude where $\partial n/\partial \theta = 0$ (not shown) was found to be 57°N , while the initial disturbance attained its maximum amplitude near 50°N (not shown). Thus, as the jet becomes stronger, there is a greater separation in latitude between where $\partial n/\partial \theta = 0$ and where the disturbance reaches its largest amplitude. As a result, to the extent that linear theory can be applied, it is not sur-

prising that a larger fraction of wave activity propagates equatorward as the jet becomes stronger.

Another interesting result is that the orientation of \mathbf{F} is different on either side of the jet. On the equatorward side of the jet, \mathbf{F} primarily has a horizontal orientation, whereas on the poleward side its orientation is vertical. This suggests that barotropic critical-layer dynamics, such as that studied by Warn and Warn (1976) and Killworth and McIntyre (1985), is relevant to the decay on the equatorward side of the jet, whereas baroclinic critical-layer dynamics applies to the poleward side of the jet.

b. Horizontal shear and stabilization

As discussed by James and Gray (1986), an increase in the barotropic part of the horizontal zonal wind shear usually modifies the structure of a growing disturbance to reduce its growth rate. In addition, they found that if the ratio of the horizontal wind shear to the Eady growth rate, $\omega_y = \partial U/\partial y/\omega_z$, where

$$\omega_z = 0.31 \frac{f \partial U/\partial z}{N},$$

is greater than 1, the growth rate of the disturbance will be significantly reduced. A latitude-time diagram

illustrating ω_y is shown in Fig. 7. For this parameter, the lowest model level is used. It can be seen that there is a reasonably good correspondence between the latitudes where the low-level meridional heat flux is large and where ω_y is small (compare the latitudes of minimum ω_y with the structure of $|F|$ in Fig. 6). As an example, at the latitude of the jet center, ω_y is small during the growth stages of both the first and the second cycles. For the second cycle, this reduction in ω_y is due to both an increase in ω_z and a decrease in $\partial U/\partial y$. After the disturbance decays, ω_y maintains fairly large values between 30°N and 60°N.

The above properties of ω_y together with the stabilization at the end of the first cycle suggest that the stabilization is due to the barotropic governor mechanism of James and Gray. To further test this idea, a procedure similar to that in James and Gray is used to remove the barotropic component of the zonal flow. In their study, the stability of the time-averaged flow was examined with the barotropic component of the zonal flow removed. In the present study, the barotropic component of the zonal flow will be removed at a particular time during the evolution of the disturbance. Then, the linear stability of this adjusted flow will be examined. This removal is accomplished by first subtracting the lowest-level zonal wind from the zonal wind at all levels and by setting the meridional wind to zero everywhere. The surface pressure field is then adjusted to a balanced state at the lowest model level. Then, using the temperature field and the new surface pressure field, a new nonlinearly balanced zonal wind field is calculated. This balanced wind field is only slightly different from the earlier wind field with the lowest-level zonal wind removed. To this adjusted wind and surface pressure field, a small amplitude perturbation is added.

The effect of horizontal shear is examined at day 60. This is at a time when the disturbance is decaying most rapidly. As expected, a linear stability analysis of the zonally averaged flow finds no unstable modes. However, when the barotropic component of the zonal wind field is removed, a linear growth rate of 0.067 day^{-1} is found. The meridional heat flux structure of the growing disturbance consists of a local maxima at the lowest levels on both sides of the jet. This result is in agreement with that of James and Gray who found the removal of the barotropic component of the zonal flow returns the linear growth rate close to its initial value.

4. Conclusions and discussion

The weakly nonlinear life cycle of a baroclinic disturbance was investigated with a multilevel, spherical primitive equation model. In this study, the weakest possible jet that gives baroclinic growth/barotropic decay life cycles was examined. Through the use of this model, additional insight has been obtained into both the wave activity propagation and stabilization char-

acteristics of both class 1 (weakly nonlinear, two-layer, β -plane quasigeostrophic) and class 2 (strongly nonlinear, multilevel, spherical, primitive equation) models. Furthermore, it was also verified that the critical surface bounds the disturbances at all times and all levels throughout the model's middle and upper troposphere.

Wave activity propagation was found to occur on both the equatorward and poleward sides of the jet, with a small preference for equatorward propagation. This contrasts all class 2 results, for example, Simmons and Hoskins (1978) and Barnes and Young (1992), where a much larger fraction of the wave activity propagates equatorward, and the class 1 results of FH and F, who found equal wave activity propagation in both directions. In FH and F, the symmetry imposed by the β -plane approximation requires that the wave activity propagation is symmetric about the jet center. Thus, it seems reasonable to assume that the difference in the direction of wave activity propagation between the present results and those in class 1 models is due to the breaking of the symmetry associated with sphericity. The greater tendency for equatorward wave activity propagation in class 2 models was examined through the use of the quasigeostrophic refractive index. It was shown that as the strength of the jet increased, a larger fraction of the disturbance was generated on the equatorward side of the $\partial n/\partial \theta = 0$ latitude, which within the limitations of linear theory, implies a further preference for equatorward wave activity propagation.

In contrast to class 1 models, and in agreement with the strongly nonlinear life cycle study of James and Gray, it was found that the stabilization of the flow was through the barotropic governor mechanism. A plausible explanation for these differences in stabilization is related to the necessary condition for instability in two-layer and multilevel models. This was discussed in the Introduction, where it was noted that the lowest-layer meridional potential vorticity gradient can easily be rendered positive in the two-layer model, but this gradient must remain negative at some latitude in the vertically continuous model. As a result, it is not surprising that the flow is stabilized by another mechanism, such as through the barotropic governor, when a sufficiently large number of vertical levels is used. The fact that the barotropic governor can play an important role in both the present model and class 2 models, and not in class 1 models, must also be related to the number of layers. In FH and F, it was found that the change to the horizontal zonal wind shear during the life cycle is relatively small. However, in multilayer models, because the low-level meridional temperature gradient cannot be removed, there must eventually be some regions of strong low-level vertical wind shear and other regions of weak vertical wind shear. As a result, strong horizontal wind shears must develop and in turn stabilize the flow through the barotropic governor mechanism.

The temporal evolution of the disturbance consisted of two large amplitude cycles, followed by a decay via diffusive processes. This multiple cycle evolution resembles that found with class 2 models, which also yield multiple life cycles. However, the growth characteristics of the second cycle were found to be very different from those seen in recent class 2 model studies such as MacVean and James (1986) and Barnes and Young (1992). MacVean and James found that the second life cycle was due to baroclinic instability associated with the low-level increase in the meridional temperature gradient at the wings of the jet. In the study of Barnes and Young, the first cycle was characterized by baroclinic growth followed by barotropic decay, whereas all subsequent cycles took on barotropic properties, as a sequence of alternating critical-level absorption and overreflection stages occurred. Consistent with this critical-level absorption and overreflection, the direction of the momentum flux changed from poleward to equatorward, respectively. The behavior found in both of these studies contrasts with the present weakly nonlinear study, where it was indicated that the second life cycle may arise from a nonmodal instability. Since the zonally averaged flow was found to be stable at the end of the first cycle, nonmodal instability is a plausible mechanism for the secondary growth. Thus, in multilevel primitive equation models, there are at least three different mechanisms through which secondary life cycles can take place.

As discussed in the Introduction, a second cycle was never found to occur in the class 1 model results of FH and F. The absorption/overreflection life cycles identified by Barnes and Young cannot occur in class 1 models, since as was indicated in FH, $\partial Q/\partial y$ must become negative in the upper layer, which can only happen if the initial jet is strongly unstable. The multiple life cycles arising from baroclinic instability at the wings of the jet, as described by MacVean and James, does not take place in class 1 models simply because the lower layer $\partial Q/\partial y$ becomes positive at the end of the first cycle.

Since the disturbance is bounded by its critical surface, and because the zonal wind speed and disturbance angular velocity do not change substantially in the model's middle and upper troposphere, the extent of meridional propagation of the disturbance could have been predicted. Whether this is possible for strongly unstable flows will depend on the magnitude of the zonal wind changes and how the angular velocity spectrum evolves. Barnes and Young found that the disturbance's mean phase speed could shift by as much as 10° latitude during a baroclinic life cycle.

The results found in the present study are expected to be quite similar to that obtained with a weakly nonlinear, multilevel, spherical, quasigeostrophic model. This is because the static stability changes must be small in a weakly nonlinear model, since the initial meridional temperature gradient is small, and it is the fixed

static stability that accounts for the main differences between primitive equation and quasigeostrophic baroclinic wave evolution.

It was also found that the location of minima in a parameter representing the ratio of the horizontal shear of the zonal wind to the Eady growth rate was a reasonable predictor as to the location of the growing disturbance at low levels. One possible explanation for this relationship is that the zonally averaged flow changes sufficiently slowly that the disturbance has time to adjust its structure. In addition, since the first cycle arose from baroclinic instability and the second cycle possibly from nonmodal instability, this parameter managed to indicate the region from which the disturbance could most easily gain energy from the background flow during both types of growth periods. It would be interesting to examine to what extent the same parameter could indicate the location of a more rapidly growing disturbance in a strongly nonlinear flow.

Acknowledgments. I would like to thank Drs. Jeffrey Barnes, Sukyoung Lee, Randy Dole, and Jeff Whitaker, and an anonymous reviewer, for their helpful comments on this manuscript, and Dr. Isaac Held both for his valuable discussions and for providing the primitive equation code that he developed. In addition, I would also like to thank Dr. Rob Black for providing an EP flux code that was used to compare the accuracy of the EP flux code developed by the author. This work was supported by the NOAA Climate and Global Change Program.

APPENDIX

Parameter Values for Initial Zonally Averaged Flow

The parameters in (2.1) are assigned the values $U_0 = 16.2 \text{ m s}^{-1}$, $H/\sigma_z = 1.07$, $\sigma_\theta = 12.5$ degrees, $a = 6.37 \times 10^6 \text{ m}$, $R = 287 \text{ J K}^{-1} \text{ kg}^{-1}$, $\theta_0 = 45 \text{ deg}$, $\sigma_0 = 0.275$, and for the Coriolis parameter f , the earth's angular velocity $\Omega = 7.292 \times 10^{-4} \text{ s}^{-1}$ is used. This form for the zonally averaged temperature field corresponds to an analytical zonal wind field in thermal wind balance that has a sech squared profile both in latitude and in geometric height if the Coriolis parameter is kept constant.

The values for $[T(\sigma)]$, which are the latitudinal and zonally averaged temperature field, are shown in Table A1. This temperature field was derived by modifying those in Oort and Rasmusson (1971) in order to specify unrealistically low temperatures in the lower levels of the model. At the lowest few levels in the model, the above initial state has an unrealistically small meridional temperature gradient. As a result, the initial state will be statically unstable in polar regions if observed values for $[T(\sigma)]$ are used. To suppress this instability, the low-level Brunt-Väisälä frequency is increased by specifying $[T(\sigma)]$ to have values smaller than those observed in the atmosphere at the model's lowest levels.

TABLE A1. Values of $[T(\sigma)]$.

| σ | $[T(\sigma)]$ (C) |
|----------|-------------------|
| 0.025 | -40.20 |
| 0.075 | -41.20 |
| 0.125 | -42.20 |
| 0.175 | -42.98 |
| 0.225 | -42.89 |
| 0.275 | -42.80 |
| 0.325 | -41.40 |
| 0.375 | -39.30 |
| 0.425 | -36.30 |
| 0.475 | -33.20 |
| 0.525 | -30.10 |
| 0.575 | -27.50 |
| 0.625 | -25.10 |
| 0.675 | -22.90 |
| 0.725 | -20.90 |
| 0.775 | -19.10 |
| 0.825 | -17.30 |
| 0.875 | -15.50 |
| 0.925 | -13.60 |
| 0.975 | -11.70 |

REFERENCES

- Andrews, D. G., and M. E. McIntyre, 1976: Planetary waves in horizontal and vertical shear, the generalized Eliassen-Palm relation and the mean zonal acceleration. *J. Atmos. Sci.*, **33**, 2031-2048.
- Barnes, J. R., and R. E. Young, 1992: Nonlinear baroclinic instability on the sphere: Multiple life cycles with surface drag and thermal damping. *J. Atmos. Sci.*, **49**, 861-878.
- Branscome, L. E., W. J. Gutowski, Jr., and D. A. Stewart, 1989: Effect of surface fluxes on the nonlinear development of baroclinic waves. *J. Atmos. Sci.*, **46**, 460-475.
- Edmon, H. J., B. J. Hoskins, and M. E. McIntyre, 1980: Eliassen-Palm cross sections for the troposphere. *J. Atmos. Sci.*, **37**, 2600-2616.
- Farrell, B. F., 1982: The initial growth of disturbances in a baroclinic flow. *J. Atmos. Sci.*, **39**, 1663-1686.
- , 1984: Modal and non-modal baroclinic waves. *J. Atmos. Sci.*, **41**, 668-673.
- Feldstein, S. B., 1991: A comparison of the weakly nonlinear instability of westerly and easterly jets in a two-layer beta-plane model. *J. Atmos. Sci.*, **48**, 1701-1717.
- , and I. M. Held, 1989: Barotropic decay of baroclinic waves in a two-layer beta-plane model. *J. Atmos. Sci.*, **46**, 3416-3430.
- Gall, R. L., 1976: Structural changes of growing baroclinic waves. *J. Atmos. Sci.*, **33**, 374-390.
- Gutowski, W. J., Jr., L. E. Branscome, and D. A. Stewart, 1989: Mean flow adjustment during the life cycles of baroclinic waves. *J. Atmos. Sci.*, **46**, 1724-1737.
- Haynes, P. H., and T. G. Shepherd, 1989: The importance of surface-pressure changes in the response of the atmosphere to zonally-symmetric thermal and mechanical forcing. *Quart. J. Roy. Meteor. Soc.*, **115**, 1181-1208.
- Hoskins, B. J., 1983: Modelling of the transient eddies and their feedback on the mean flow. *Large-Scale Dynamical Processes in the Atmosphere*, B. J. Hoskins and R. P. Pearce, Eds., Academic Press, 169-199.
- James, I. N., 1987: Suppression of baroclinic instability in horizontally sheared flows. *J. Atmos. Sci.*, **44**, 3710-3720.
- , and Hoskins, 1985: Some comparisons of atmospheric internal and boundary baroclinic instability. *J. Atmos. Sci.*, **42**, 2142-2155.
- , and L. J. Gray, 1986: Concerning the effect of surface drag on the circulation of a baroclinic planetary atmosphere. *Quart. J. Roy. Meteor. Soc.*, **112**, 1231-1250.
- Killworth, P. D., and M. E. McIntyre, 1985: Do Rossby-wave critical layers absorb, reflect or over-reflect? *J. Fluid Mech.*, **161**, 449-492.
- Lindzen, R. S., 1988: Instability of plane parallel shear flow (toward a mechanistic picture of how it works). *Pure Appl. Geophys.*, **126**, 103-121.
- Lorenz, E., 1955: Available potential energy and the maintenance of the general circulation. *Tellus*, **7**, 157-167.
- MacVean, M. K., and I. N. James, 1986: On the differences between lifecycles of some baroclinic waves using the primitive and quasi-geostrophic equations on a sphere. *J. Atmos. Sci.*, **43**, 741-748.
- Oort, A. H., and E. M. Rasmusson, 1971: Atmospheric circulation statistics. N.O.A.A. Prof. Paper 5, U.S. Dept. of Commerce.
- Palmer, T. N., 1982: Properties of the Eliassen-Palm flux for planetary scale motions. *J. Atmos. Sci.*, **39**, 992-997.
- Pedlosky, J., 1970: Finite-amplitude baroclinic waves. *J. Atmos. Sci.*, **27**, 15-30.
- , 1971: Finite-amplitude baroclinic waves with small dissipation. *J. Atmos. Sci.*, **28**, 587-597.
- , 1981: The effect of β on the chaotic behavior of unstable baroclinic waves. *J. Atmos. Sci.*, **38**, 717-731.
- , and C. Frenzen, 1980: Chaotic and periodic behavior of finite-amplitude baroclinic waves. *J. Atmos. Sci.*, **37**, 1177-1196.
- Polavarapu, S. M., and W. R. Peltier, 1990: The structure and nonlinear evolution of synoptic scale cyclones: Life cycle simulations with a cloud scale model. *J. Atmos. Sci.*, **47**, 2645-2672.
- Randel, W. J., and J. L. Stanford, 1985: An observational study of medium-scale wave dynamics in the Southern Hemisphere summer. Part I: Wave structure and energetics. *J. Atmos. Sci.*, **42**, 1172-1188.
- , and I. M. Held, 1991: Phase speed spectra of transient eddy fluxes and critical layer absorption. *J. Atmos. Sci.*, **48**, 688-697.
- Simmons, A. J., and B. J. Hoskins, 1978: The life cycles of some nonlinear baroclinic waves. *J. Atmos. Sci.*, **35**, 414-432.
- , and —, 1980: Barotropic influences on the growth and decay of non-linear baroclinic waves. *J. Atmos. Sci.*, **37**, 1679-1684.
- Snyder, C. M., and R. S. Lindzen, 1988: Upper-level baroclinic instability. *J. Atmos. Sci.*, **45**, 2445-2459.
- Thorncroft, C. D., and B. J. Hoskins, 1990: Frontal cyclogenesis. *J. Atmos. Sci.*, **47**, 2317-2336.
- Warn, T., and H. Warn, 1978: The evolution of a nonlinear critical level. *Stud. Appl. Math.*, **59**, 37-71.